Wigner functions for the diamagnetic hydrogen atom: quantum fringes

1994 J. Phys. A: Math. Gen. 27 787

(http://iopscience.iop.org/0305-4470/27/3/021)

J. Phys. A: Math. Gen. 27 (1994) 787–800. Printed in the UK

Wigner functions for the diamagnetic hydrogen atom: quantum fringes

T S Monteiro

Department of Mathematics, Royal Holloway University of London, Egham, Surrey TW20 0EX, UK

Received 28 July 1993

Abstract. Phase-space distributions (Wigner functions) for eigenstates of the diagmagnetic hydrogen atom at fixed scaled energy have been obtained for the intermediate regime in between regularity and full chaos. States localized on the three major fixed points of the classical Poincare surface of section have been considered. While previous numerical work was primarily concerned with phase-space localization on period orbits, here the oscillatory structure (quantum fringes) forms the main subject. The fringes are delocalized relative to the dominant positive structures. Although the latter are strongly localized on fixed points and their associated invariant manifolds, the fringes permeate the whole energy surface. Fringes originating in the ergodic part of phase-space experience an abrupt change in character, in addition to the expected fall in amplitude, within stable islands. As a result, a single quantum state can provide a striking map of the global structure of phase-space. Phase-space is partitioned into relatively strong irregular scar fringes in the ergodic region and weaker regular Airy type fringes inside stable islands. Quantum probability distributions near bifurcations and confluences have also been examined. A comparison with Husimi distributions has been carried out and it is shown that the latter have lost some dynamically interesting structures.

1. Introduction

The Poincaré surface of section (SOS) has played a preeminent role in studies of the classical dynamics of systems which exhibit 'soft chaos'. These systems experience a gradual transition from integrable to chaotic motion, as some parameter is varied (Gutzwiller 1990). Consequently there is an intermediate regime between completely integrable motion, where phase space is densely filled with tori, and chaos, where ergodic trajectories fill the whole energy surface on the SOS.

In between these extremes, stable islands coexist with ergodic regions in a mixed phase space. Here the KAM theorem regulates the break-up of tori near resonances into chains of elliptic islands and unstable fixed-points. This process recurs on increasingly finer scales—indeed structure on infinitely fine scales is one of the hallmarks of classical chaos. It is the quantum behaviour in this intermediate regime which concerns the work here. For a quantum system the Heisenberg uncertainty principle precludes simultaneous knowledge of momentum and position, p and q, on scales finer than Planck's constant $\hbar$, placing a limit on quantum representations of the classical SOS.

Nevertheless there has been extensive work on quantum phase-space probability distributions and their relation to the classical SOS. Two particular examples have been

0305-4470/94/030787+14$07.50

singled out: the Wigner distribution and the related Husimi distribution (see Hillery *et al* 1984 for a comprehensive review of their properties).

In brief, the Wigner function for a given eigenstate i (Wigner 1932) is the Weyl transform of the wavefunction and is obtained from the wavefunction as follows:

$$W_i(\boldsymbol{p}, \boldsymbol{q}) = 1/(2\pi\hbar)^N \int \Psi_i^*(\boldsymbol{q}+\lambda/2)\Psi_i(\boldsymbol{q}-\lambda/2) \exp(-\mathrm{i}\boldsymbol{p}\cdot\lambda/\hbar)\, \mathrm{d}^N\lambda.$$

It is normalized as

$$\int W_i(\boldsymbol{p}, \boldsymbol{q})\, \mathrm{d}^N\boldsymbol{p}\, \mathrm{d}^N\boldsymbol{q} = 1$$

and is orthogonal for different eigenstates.

In addition, when projected down the p or the q axis it yields the probability density in the position or momentum representation, respectively. These requirements mean that it cannot be positive everywhere, a perceived drawback for its interpretation as a probability distribution. In fact it oscillates within the energy surface with spacing dependent on $\hbar$ making its graphical representation more difficult. For this reason, attempts to represent it, for all but the simplest cases, have to date been limited to the strongest structures. Previous numerical investigations concentrated on phenomena such as localization on tori or fixed points (Schweizer *et al* 1993, Jans *et al* 1993). Here the fringes and associated negative probability were little more than an embarrassment and since in the regular to intermediate regime they are quite weak, they could easily be overlooked, particularly if they were evaluated by means of a numerical Fourier transform.

Wigner functions were investigated theoretically for the integrable regime by Berry (1977) and Ozorio de Almeida and Hannay (1982). They were shown to be peaked on tori but 'decorated' by an oscillatory pattern of fringes. Within tori, a semiclassical approximation by Berry (1977), predicted an Airy pattern of oscillations. Berry (1989a) also showed that in the ergodic limit an Airy pattern on the energy surface is recovered from the contribution of short period orbits if the periodic orbits are damped out by smoothing over a limited energy range. However, there has been much interest over the last decade in the probability enhancements (scars) due to unstable periodic orbits (Heller 1984).

For studies of these scars, the alternative probability distribution, the Husimi distribution, has proved most popular (Geisel *et al* 1986, Leboeuf and Saraceno 1990, Muller 1992, Muller *et al* 1993). It is obtainable from the overlap between the wavefunction and a coherent state, and effectively represents a Gaussian smoothing of the Wigner function. Takahashi (1989) has discussed many of the relative advantages of the Husimi distribution over the Wigner function. Principally the Husimi is positive definite and the smoothing out of the oscillatory structure will make the classical limit better behaved. However, the Husimi distribution does depend significantly on the smoothing width adopted (de Aguiar and Ozorio de Almedia 1990). It is shown below by comparison of numerical results, that, though less troubling to interpret as a probability distribution, the Husimi smoothing may remove interesting dynamical information for finite values of $\hbar$ which is readily apparent in the Wigner function.

Hutchinson and Wyatt (1980) investigated the Wigner distributions for the Henon–Heiles Hamiltonian. They reported only the strongest few 2-d contours on the sos, which showed that individual states were localized on tori in the regular regime but

relatively more spread-out in ergodic regions. Schweizer *et al* (1993), Jans *et al* (1993) and Monteiro (1992) examined localization on periodic orbits for diamagnetic atoms and molecules. In Monteiro (1992), wavefunctions for a Rydberg molecule were obtained by the *R*-matrix method in the form of an expansion over Sturmian functions. These were then transformed into scaled semi-parabolic coordinates $\mu, \nu = (\zeta/2(r \pm z))^{1/2}$ where ζ is the Sturmian parameter, and thence to an expansion over coupled one-dimensional harmonic oscillator states:

$$\Psi = \sum C_{mn} H_m(\mu) H_n(\nu) \exp -(\nu^2 + \mu^2)/2.$$

The Wigner functions are then given analytically. Hence the Wigner function can be calculated to high accuracy. The hydrogen atom was investigated here using the same procedure—the wavefunction is much simpler to calculate than those of non-hydrogenic systems since it is obtained by direct diagonalization of the Hamiltonian in a basis of Sturmians (Clark and Taylor 1982) and can even be obtained directly in a basis of two-dimensional harmonic oscillator states (Wintgen and Friedrich 1986).

The problem of the hydrogen atom in a strong magnetic field has proved exceptionally suitable in studies of soft chaos. A scaling transformation of the position and momentum $p \to p\gamma^{1/3}$ $r \to r\gamma^{-2/3}$ makes the classical Hamiltonian dependent only on a single parameter, the scaled energy, $\varepsilon = E\gamma^{-2/3}$. The dynamics undergo a transition from integrability to full chaos as ε ranges from $-\infty$ to 0. The Hamiltonian in scaled semi-parabolic coordinates takes the form for $l_z = 0$:

$$H = (p_\mu^2 + p_\nu^2)/2 - \varepsilon(\nu^2 + \mu^2) + (1/8)(\nu^2\mu^4 + \mu^2\nu^4) = 2.$$

In figure 1 a set of classical sos taken through the $\mu = 0$ plane, obtained by Schweizer *et al* (1988), have been reproduced for comparison with the quantum results. The problem of the diamagnetic hydrogen atom has been extensively reviewed elsewhere (Hasegawa *et al* 1989, Friedrich and Wintgen 1989). However, for the features of interest here the details of atomic physics are not central, so the problem will be simply described in terms of its classical surfaces of section, which share many general characteristics of Hamiltonian systems with soft chaos.

The Poincaré sos show the transition to chaos. Figure 1 shows that for $\varepsilon = -1$, phase-space is filled with tori. There are three major fixed points indicated in figure 1 as V1, R1 and C (using the notation of Holle *et al* 1988, where orbits were associated with 'vibrator' (V) or 'rotator' (R) quantum states).

The elliptic fixed point at the centre of the section (V1) corresponds to a periodic orbit parallel to the magnetic field. The other major elliptic fixed point (R1) at the centre of the two other islands corresponds to a periodic orbit perpendicular to the magnetic field. Finally the hyperbolic fixed point on the separatrix between the islands corresponds to a near-circular (C) unstable periodic orbit. The surfaces of section show that chaotic trajectories gradually spread out around the C fixed point. The central island vanishes near $\varepsilon = -0.39$, where the orbit parallel to the field (V1) becomes unstable. At energies $\varepsilon > -0.127$ the island centred on R1 is destroyed and the sos is completely filled by ergodic trajectories. These short-period classical periodic orbits are responsible for well studied modulations of the energy level spectrum of hydrogen, R1 in particular being responsible for the observed quasi-Landau modulations of the photoabsorption spectrum of diamagnetic Rydberg atoms.

The quantum picture is slightly more complicated. The scaling transformation can still be carried out and it is possible to calculate spectra of levels corresponding to a fixed scaled energy, i.e. corresponding to a given classical regime (Wintgen and Friedrich

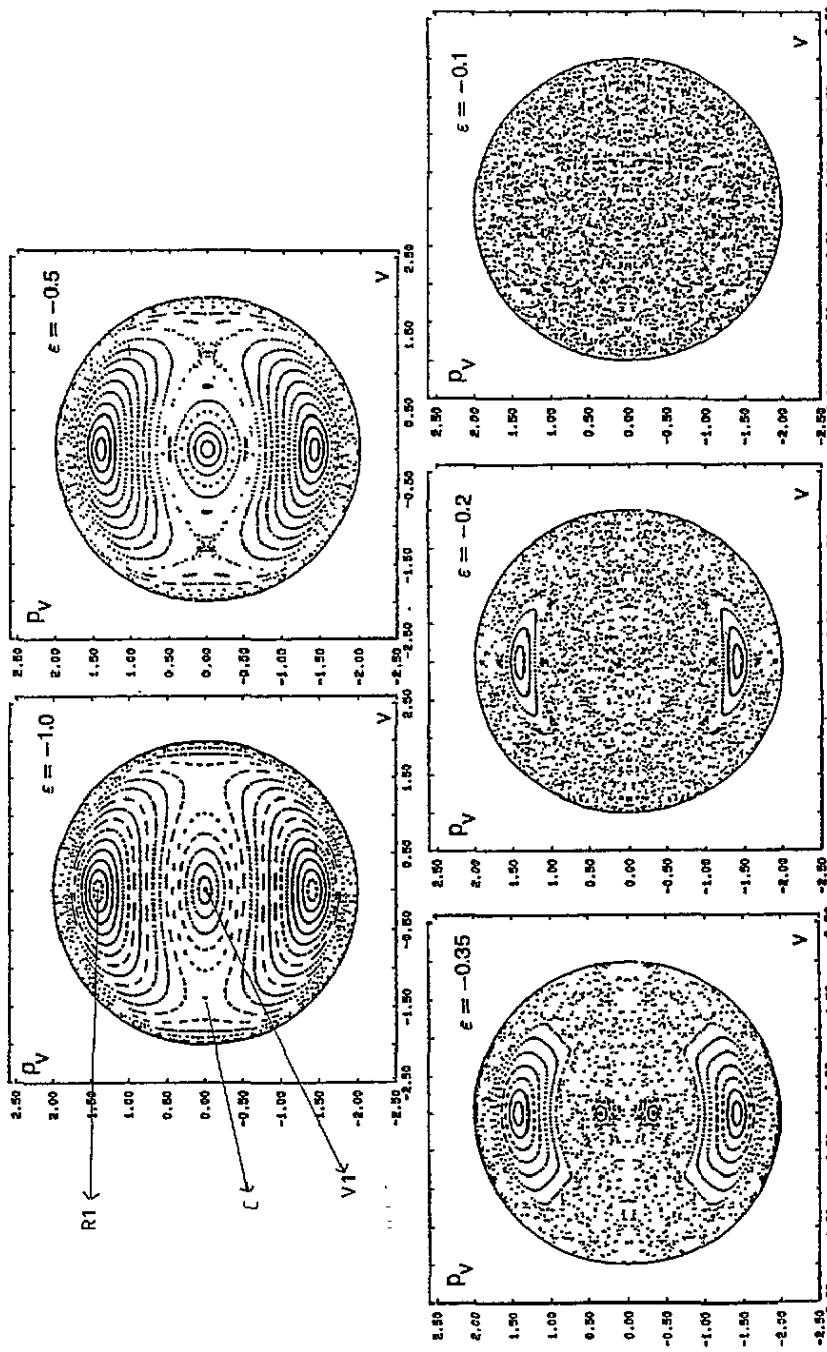

Figure 1. Classical Poincare surfaces of section ($u=0$) for the H atom in a magnetic field, at fixed scaled energies $-1 \leqslant \varepsilon \leqslant -0.1$ for zero magnetic quantum number from Schweizer *et al* (1988). u, v are semiparabolic coordinates $=(r \pm z)^{1/2}$. The first figure indicates the three fixed points (R1, V1, C) considered here.

1987). However each level will correspond to a different effective value of $\hbar$. In scaled coordinates, the usual quantization condition $S=\int p\,dq=n\hbar$ becomes $S=\gamma^{-1/3}\int p\,dq=\gamma^{-1/3}\int p\,dq=\gamma^{-1/3}S(\varepsilon)$; i.e. the scaled action $S(\varepsilon)=n\,\gamma^{1/3}\hbar$. In atomic units ($\hbar=1$) there is an effective value of $\hbar=\gamma^{1/3}$. So higher energy levels (corresponding to smaller γ for fixed ε) approach the semiclassical $\hbar\to 0$ limit.

In the lower energy regular regime, the energy levels supported by the large stable islands are approximately given by the quantization of Miller (1975) for an isolated stable orbit. Summing all traversals of such an orbit gives rise to a set of harmonic oscillator-like energy levels. For the diamagnetic hydrogen atom they may be characterized by two quantum numbers n, K, i.e. $S(\varepsilon)\approx n\gamma^{1/3}+(K+1/2)\alpha+\beta(\pi/2)$ where here α is the winding number of the orbit and β the Maslov index.

2. Results

Figures 2(a)–(f) represent the pattern typical of the regular regime. It shows a set of Wigner functions (same coordinates as figure 1) for neighbouring energy levels at $\varepsilon=-0.5$ associated with the perpendicular orbit (R1). Figure 2(a) shows the 185th level above the ground state, which corresponds to $K=0$ and shows localization on the elliptic fixed point of R1. Figures 2(b)–(f) represent, in sequence, levels 180, 188, 183, 187, 184. They show localization on progressively larger tori (i.e. larger values of K) centred on the fixed point, converging on the separatrix. The action taken around the loop of the torus differs (roughly) by integer values of the winding number. At this energy the parallel orbit (V1) also gives rise to a similar sequence of concentric tori.

A selection from both sets of these tori was shown in Jans *et al* (1993). However in that case the fringes were not obtained since the Wigners were calculated numerically. Only the strongest 99% or so of the probability density was calculated so only the tori were shown. However, in figure 2 all the fringes are shown, by plotting all the positive structure. White indicates negative values within the energy surface, and zero outside, since the Wigner function beyond the energy surface was not calculated for any of the states considered here.

The pictures show a phase-space permeated by regular, evenly spaced oscillations. The Wigners are plotted on a linear scale, using 10 colour 'bins', with the lightest grey shade containing the lowest 10% in intensity but with a cut-off 10^{-9} of the maximum. Hence this lowest bin can encompass variations in intensity of several orders of magnitude. Outside the tori the fringes are extremely weak, especially fringes outside the smaller tori. The weakest oscillations are those outside the central fixed point of figure 2(a), where the oscillations are 10^{-6}–10^{-7} of the maximum. Within tori the fringes are stronger and there is a characteristic pattern of concentric rings which may be compared with the Airy fringe pattern predicted by Berry (1977). These levels correspond to effective values of $\hbar\approx 0.035$. In comparison, the total phase space area in the box $=4^2$. This fringe pattern repeats itself in other parts of the spectrum and is very much a characteristic of the particular torus. The patterns are, however, parity dependent. For example, within odd-parity tori, two sets of concentric circles rather than just the one in figure 2 are apparent.

There is of course a gradual evolution with decreasing h as the number of tori supported by each island increases. The number of concentric rings in each torus depends on its K value, with the largest number associated with the separatrix state. Figure 3(a) and 3(b) show two Wigners for the separatrix state at $\varepsilon=-1$ corresponding

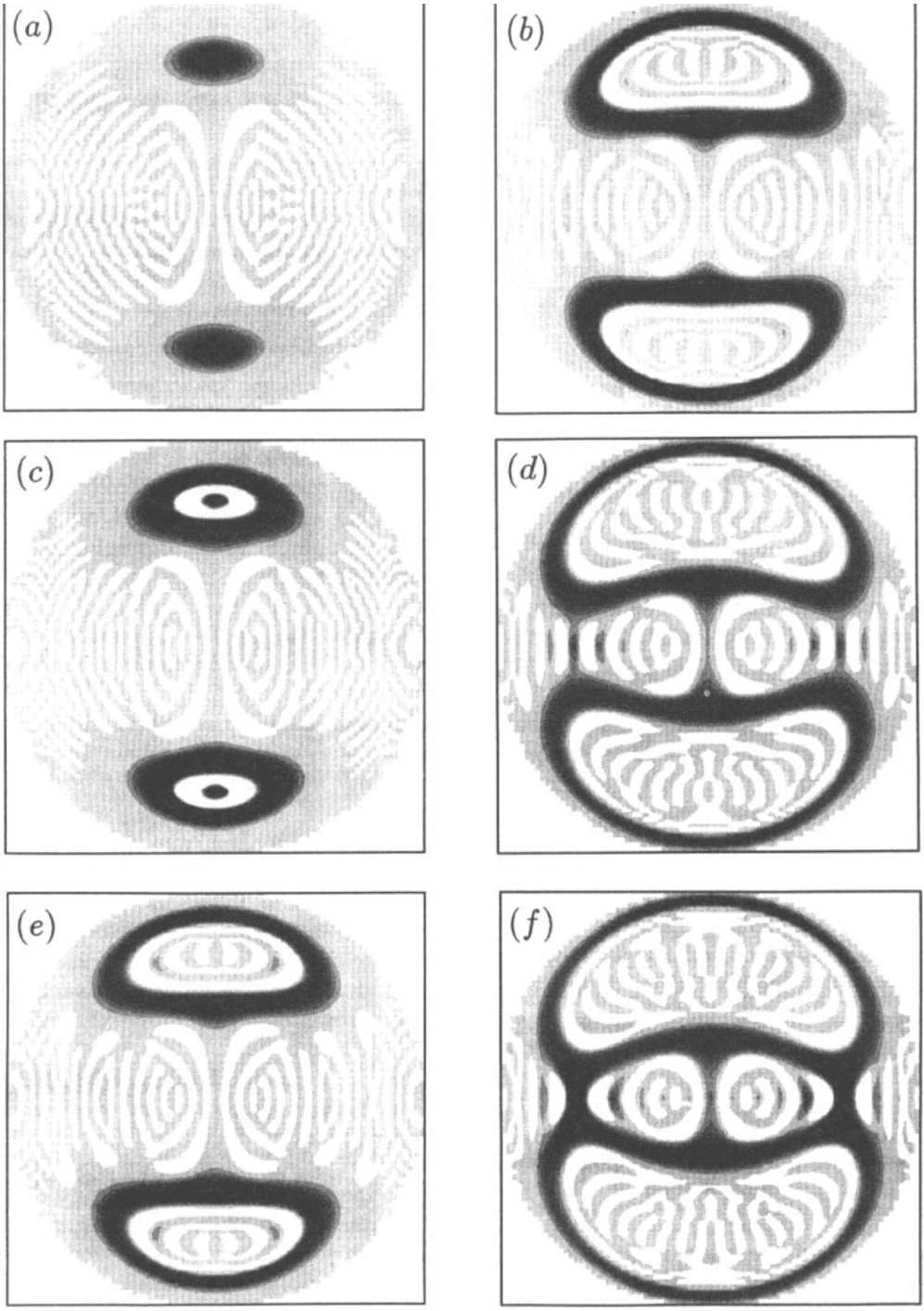

Figure 2. Wigner functions (similar coordinates to figure 1) for a set of diamagnetic hydrogen atom quantum states associated with the stable periodic orbit perpendicular to the magnetic field (R1) for $\varepsilon = -0.5$. White indicates negative values inside the energy surface and zero outside: (*a*) 185th level; (*b*) 180th level; (*c*) 188th level; (*d*) 183rd level; (*e*) 187th level; (*f*) 184th level.

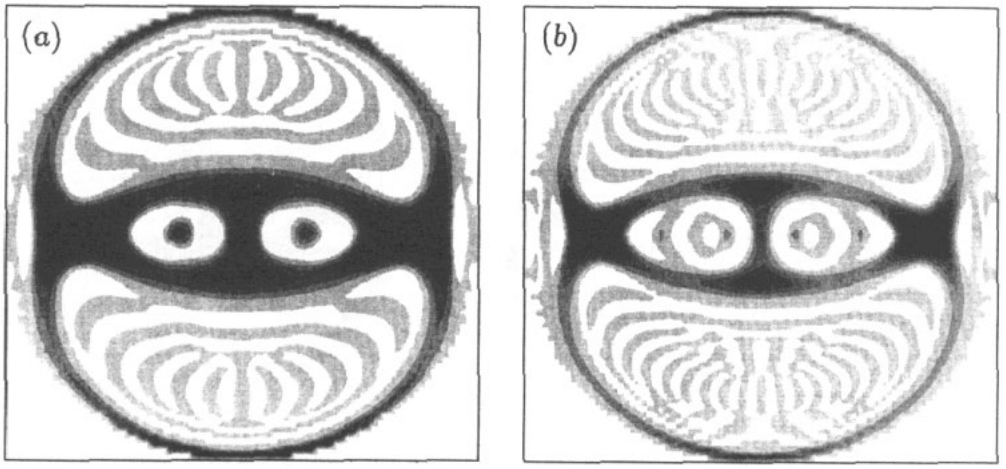

Figure 3. Wigner functions for two quantum states at $\varepsilon=-1$ associated with the near circular orbit (C), showing variation of fringe spacing with $\hbar$: (*a*) 75th state ($\hbar=0.041$); (*b*) 215th state ($\hbar=0.024$).

to the near circular orbit C. Figure 3(*a*) is level 75 above the ground state, corresponding to $\hbar=0.041$. Figure 3(*b*) is level 215 corresponding to $\hbar=0.024$. Regular fringes cover both sides of the separatrix which at this energy is bounded by stable islands on either side.

Away from the regular regime, the fringe character changes dramatically. Below, the three major fixed points are discussed separately:

The unstable fixed point C. The evolution of the fringes is shown in figure 4. Three states which are predominantly localized on C for different values of the energy ($\varepsilon=-0.5$, -0.4 and -0.3, respectively) and $\hbar\approx 0.03$–0.04 are shown. The left-hand side shows the *strong positive* structure, i.e. only the strongest 90% of the positive probability distribution (the scale is the same, with black corresponding to the same probability for all three Wigners). On the right *all* the Wigner function is shown on a scale amplified by a factor of 10^3. In the latter case, zero values outside the energy surface are indicated in grey in order to emphasize negative structures, which are cast in white.

The figures on the left show that the positive values of the quantum phase-space distribution are strongly localized on the classical hyperbolic fixed point and its invariant manifolds. The fringes however fan out to fill the whole of phase-space. In figure 4(*a*) ($\varepsilon=-0.5$) the central island is still large and the fringes are regular (i.e. similar to the Airy patterns inside tori) on both sides of the separatrix. However, as the ergodic region spreads and the islands of stability shrink there is a sharp change in character between the oscillations within and outside the stable islands. Within the ergodic region the fringes are relatively strong, but form complex patterns; these stronger oscillations associated with the unstable periodic orbit are referred to as scar fringes below.

However, inside the stable islands there are oscillations which are not simply weaker versions of the scar fringes. They are still of regular, evenly spaced character. Since these are not the obviously associated with periodic orbit scar, they are referred to as island fringes below. The result in figure 4 is quite a striking 'map' of the global structure of phase-space.

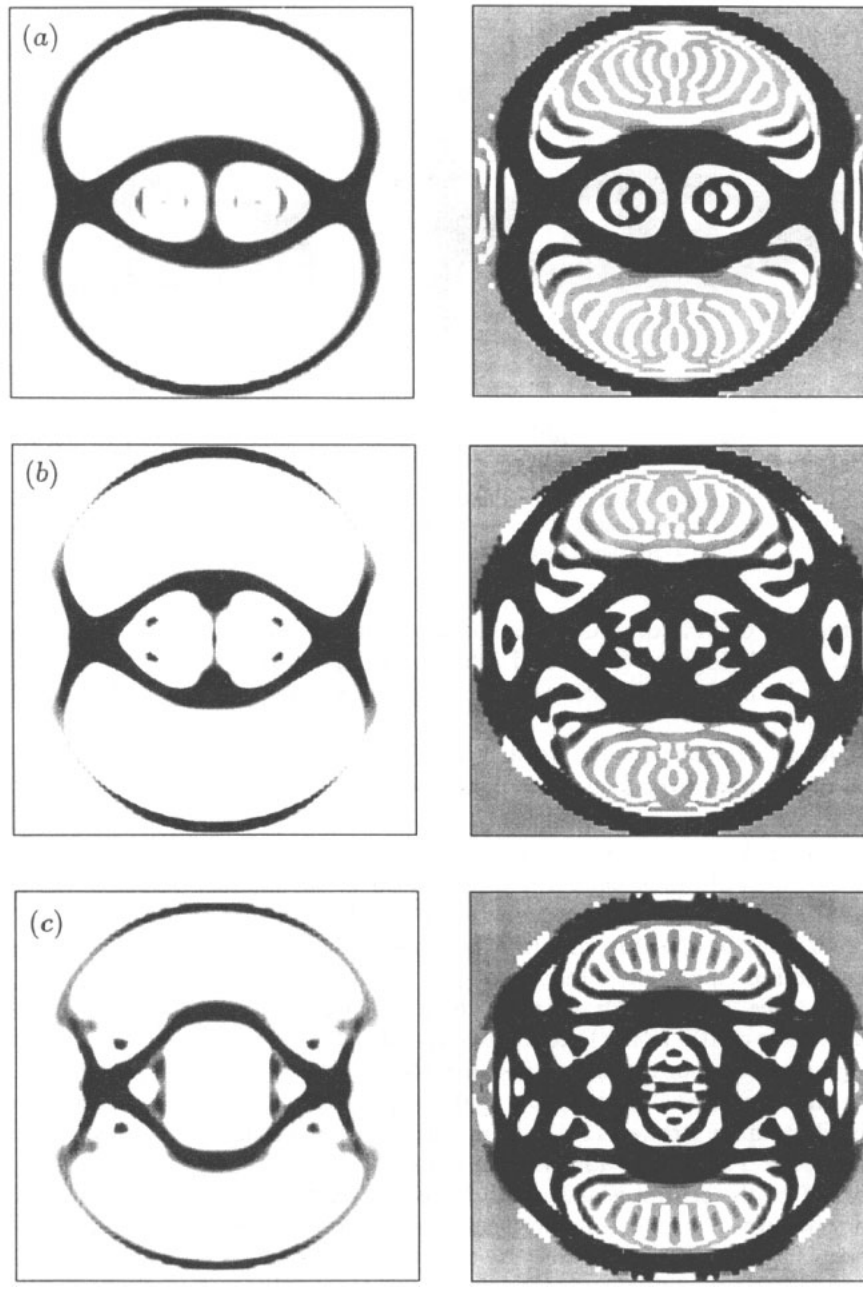

Figure 4. Wigner functions (similar coordinates to figure 1) for states associated with the scar of the unstable near-circular periodic orbit (C) showing the clear division of phase space by scar fringes in the ergodic region and island fringes inside stable islands. On the left hand side only the strongest 90% of the positive probability is plotted showing localization on the hyperbolic fixed point and invariant manifolds (black $\equiv 1$ in arbitrary units). On the right-hand side an enhanced scale (black $\equiv 10^{-3}$) is used. Grey outside the energy surface $\equiv 0$, white inside the energy surface $\equiv$ negative values: (*a*) $\varepsilon = -0.5$ (level 182, $\hbar = 0.035$); (*b*) $\varepsilon = -0.4$ (level 156, $\hbar = 0.04$); (*c*) $\varepsilon = -0.3$ (level 210, $\hbar = 0.039$).

There are large variations in fringe intensity. For figure 4 the scar fringes are 2–3 orders of magnitude weaker than the maximum, and the island fringes are in turn about 1–2 orders of magnitude weaker in turn than the scar fringes. In the semiclassical limit, the regular island should be empty as the motion is excluded by classical barriers. However, for finite $\hbar$ dynamical tunnelling through such phase-space barriers is allowable (Davies and Heller 1981). For a given ε the fringes within the stable islands were found to decrease in strength with decreasing $\hbar$, though this was not investigated quantitatively here.

It is also possible to follow a given state as ε is increased (i.e. keeping $S(\varepsilon)/\gamma^{1/3} \approx n$ constant. The fringes then become stronger as the island of stability shrinks. The general progression is for the island fringes closest to the ergodic region to become enhanced and then to be engulfed by the scar fringes. In fact the spread of scar fringes is accompanied by a rapid increase in the ratio of the volume of 'negative probability' relative to total probability of the Wigner function (insofar as we may be allowed to interpret the Wigner function as a probability distribution!) integrated over the energy surface. This provides a sort of indicator for the 'ergodicidity' of a quantum state: for low values of ε, the ratio is typically less than 1% (e.g. for R1 in figure 2(*a*) it is about 10^{-4}). As a wavefunction becomes more delocalized for higher values of ε it approaches a value of the order of unity. Of course the difference between positive and negative intensities must remain equal to unity throughout since the Wigner function is normalized. A meaningful comparison with the volume of phase-space occupied by chaotic orbits would have to take in the whole of phase-space, not just an arbitrary surface of section, and would be computationally expensive, since each Wigner surface of section here required about 30 minutes on a large mainframe (a Convex 3840 or Cray-YMP).

The stable/unstable periodic orbit V1. The periodic orbit parallel to the magnetic field experiences a series of bifurcations for $\varepsilon > -0.392$, becoming unstable over limited energy intervals but recovering stability intermittently. Well below the first bifurcation the periodic orbit is stable and the states with $K=0$ are strongly localized on the elliptic fixed point of the central island, but surrounded by a weak background of island fringes. As the ergodic region around C grows, the scar fringes spread into the ergodic region (here the term 'scar' is used loosely since the orbit is still stable). Above the bifurcation the strong localization is not only on the hyperbolic fixed point but also on the invariant manifolds.

Figure 5 shows two Wigner functions for the V1 orbit, using the same scale and the same parameters as figure 3 (except that for the representation of the strong positive structures on the left-hand side only the lowest 5% is cut off). Figure 5(*a*) illustrates the behaviour of states near the bifurcation point. It represents the 208th state above the ground state ($\hbar = 0.036$) for $\varepsilon = -0.4$. Like other $K=0$ states near the bifurcation point it exhibits very broad localization about the invariant manifolds (the diagonal structures in the centre of figure 5(*a*)). Berry (1989) calculated the form of fringes near an unstable fixed point and found that they would take the form of hyperbolae with the invariant manifolds as asymptotes. The fringe spacing was estimated as $PQ/\hbar \tanh \lambda$ in coordinates P, Q where the stability matrix is diagonal and with eigenvalues $\exp \pm \lambda$. Hence at the bifurcation, where $\lambda \to 0$ semiclassically the fringe spacing will diverge. The quantum fringes become very broad as seen in figure 5. At higher energies $\tanh \lambda \to 1$ and the spacing tends to a finite value $\sim \hbar^{1/2}$. This would suggest that it may be possible to obtain an indication of the stability of a classical orbit from the width of Wigner fringes, but this possibility has not been quantitatively examined here—at the

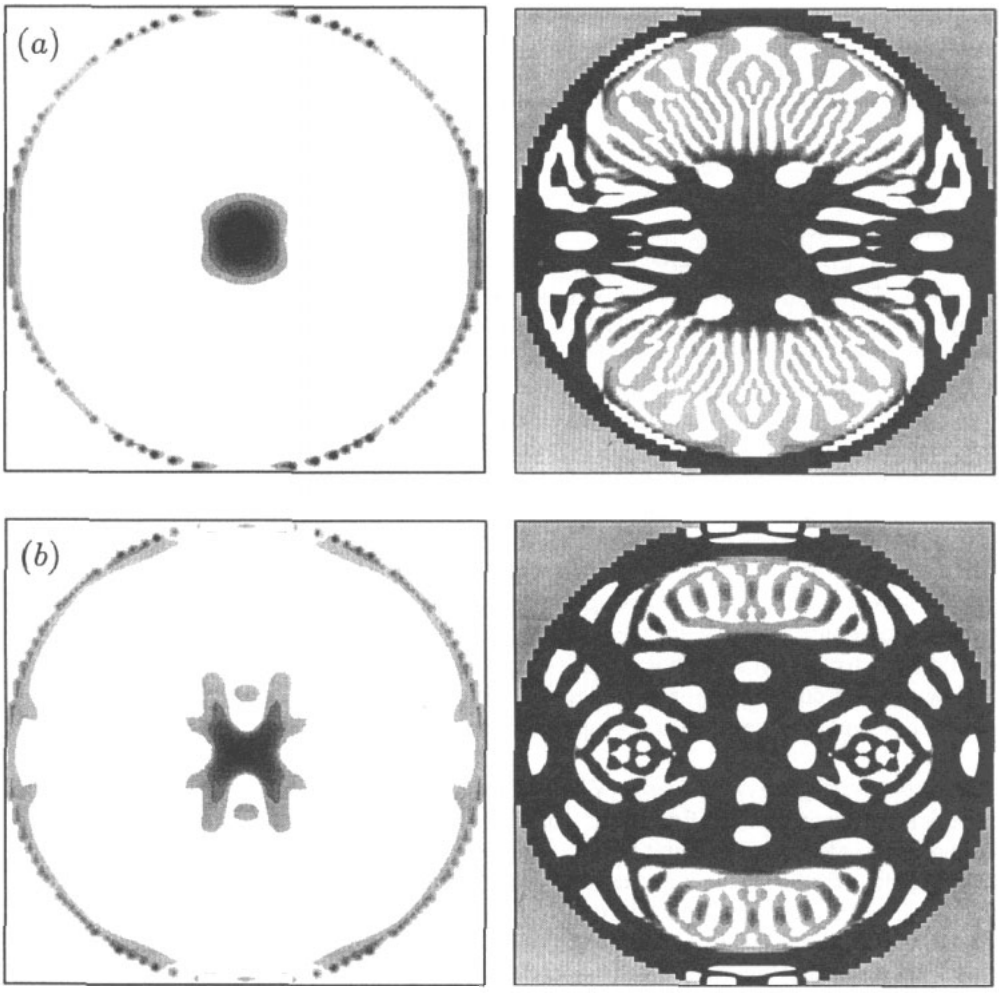

Figure 5. Wigner functions (same scales and coordinates as figure 4) for states associated with the orbit parallel to the field (V1). Left-hand side shows only strongest 95% of the positive probability. The right-hand side shows localization of the fringes on a scale enhanced by a factor of 1000: (*a*) 208th state near the first bifurcation energy where fringe widths are predicted to diverge; (*b*) 207th state near confluence energy.

values of h used here there is still considerable variation in the degree of delocalization of neighbouring $K=0$ states of the V1 series. Classically, V1 recovers stability over narrow energy ranges for $-0.392<\varepsilon<0$ but at these values of $\hbar$, V1 retains the character of an unstable orbit (e.g. localization on invariant manifolds) throughout, for $\varepsilon>-0.4$.

Figure 5(*b*) shows the 207th state ($\hbar=0.039$) for $\varepsilon\approx-0.316$. The same general pattern is apparent. The wavefunction is still strongly localized (>95%) on the fixed points and invariant manifolds. However, scar fringes fill all the ergodic region and island fringes now of magnitude 10% or so of the scar fringes are present in the stable islands. This scaled energy is especially interesting since there is a confluence associated with the perpendicular orbit (R1) which here has a rational winding number. The

confluences are discussed further below, but essentially one has the stable island surrounded by a chain of four elliptic islands interspersed by four hyperbolic fixed points. The scar fringes in figure 5(*b*) in actual fact remain well confined not only outside the stable island but also outside the island chain—as may be seen by a comparison with figure 6(*a*) (or *a* by comparison with the classical SOS at this energy which is shown in figure 6(*c*)).

The stable periodic orbit R1. The periodic orbit perpendicular to the magnetic field remains stable up to $\varepsilon=-0.127$. The elliptic fixed point at the centre of the island is associated with single quantum states given by the Millar quantization up to near that energy. The low energy pattern is illustrated in figure 2(*a*) and shows strong localization on the fixed point surrounded by very weak ($<10^{-6}$ of maximum) island fringes. One would expect this strong localization to persist while the fixed point is surrounded by an island of size $\gg\hbar$. However, here confluences studied by Schweizer *et al* play an interesting role.

Schweizer *et al* (1992) found that when the orbit R1 has a rational winding number, for scaled energy $\varepsilon=\varepsilon_{\text{con}}$ a confluence occurs and an unstable periodic trajectory disappears. One can represent this process on the classical Poincaré map. Initially, at energies slightly below ε_{con}, an island chain surrounds the central island of stability. Gradually, as the scaled energy approaches ε_{con} the hyperbolic fixed points approach the central elliptic fixed point, finally being absorbed at the confluence energy.

For $\varepsilon=-0.316$ the winding number is $\frac{3}{2}$. Figures 6(*a*) and 6(*b*) show the Wigner function 203rd level above the ground state ($\hbar=0.039$). Figure 6(*b*) shows only the strong positive structure, while figure 6(*a*) shows the whole Wigner function on an enhanced scale. In Figure 6(*c*) the classical Poincaré surface of section $\varepsilon=-0.316$, taken from Dando *et al* (1993) is shown for comparison. Finally, the corresponding Husimi distribution evaluated by taking the overlap with a coherent state is shown in figure 6(*d*). For a basis of coupled one-dimensional harmonic oscillators the overlap with a coherent state takes a particularly simple form (Lebouef and Saraceno 1990) and for the states considered here it was at least an order of magnitude faster to evaluate than the Wigner function.

It may be seen from figures 6(*a*) and 6(*c*) that the Wigner function matches remarkably the form of the classical Poincaré map at this energy. The elliptic islands of the chain appear as relatively strong negative features, while positive probability is concentrated in the central island as well as on the hyperbolic fixed points and their manifolds. The boundaries of the localization are now provided not by the central stable island but by the surrounding island chain—consistent also with figure 5(*b*), where the major phase space barrier is not the central stable island but the island chain surrounding it. Outside this barrier the island fringes have been completely replaced by the scar fringes. It must be said though that it is not clear at this point whether the barrier to the spread of probability from the central fixed point (or into the stable island in the case of figure 5(*b*)) is actually the island chain itself or some other phase-space structure such as a cantorus bordering it.

The Husimi distribution, on the other hand, shows no trace of the island chain at all. Figure 6(*d*) has been plotted with a cut-off 1/1000th of maximum, so that the weakest contour would correspond to the outline of the island chain in figure 6(*a*), (i.e. the black structure in figure 6(*a*)). The Gaussian smoothing has averaged out completely the alternating positive/negative structures, leaving simply a distorted outline. The

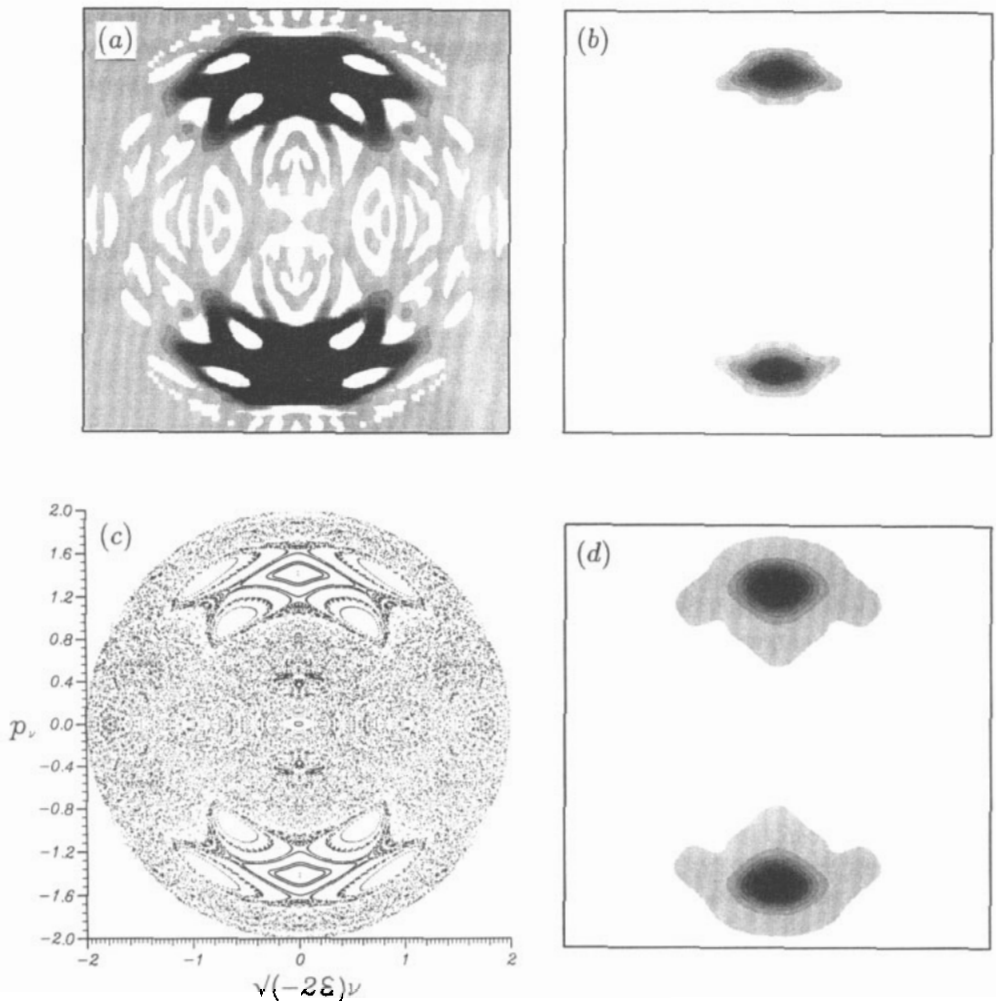

Figure 6. Quantal and classical phase-space near a confluence energy $\varepsilon = -0.316$ (winding number of periodic orbit $R1 = \frac{3}{2}$) where the main elliptic island is surrounded by an island chain: (*a*) Wigner function of 203rd state showing the island chain; (*b*) strongest positive structures of Wigner function; (*c*) Classical Poincaré surface of section; (*d*) Husimi function of 203rd state showing that the island chain has been eliminated.

Husimi distribution is more akin to the strongest Wigner structures, which are shown in figure 6(*b*).

Figure 7 shows the Wigner functions (figure 7(*a*)) and Husimi distribution (figure 7(*b*)) of the 206th level for $\varepsilon = -0.21$, another confluence energy. However, here the winding number is $\frac{4}{3}$ so in this case there is a chain of six elliptic and six hyperbolic fixed points surrounding the central elliptic fixed point and the rest of phase-space is almost all filled by chaotic orbits. Also it is worth noting that at this energy there is already a significant number of unstable periodic orbits and that finding states where a single scar strongly dominates a given quantum state is becoming progressively more difficult. However, for level 206, once again the Wigner function shows an island chain of the same form as that present in the classical sos, manifested in the form of alternating

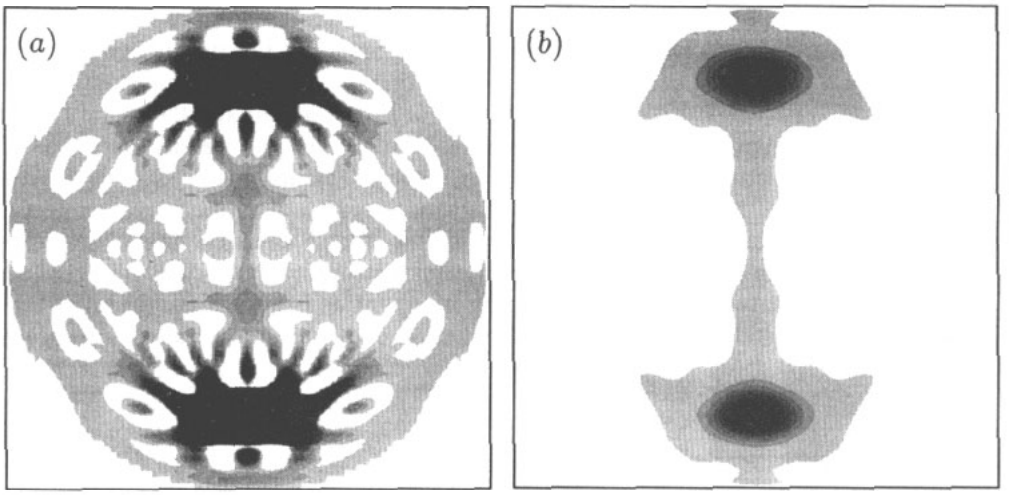

Figure 7. 206th state at the confluence energy $\varepsilon=-0.21$ (winding number of R1 $=\frac{4}{3}$. Classically the main stable island centred on R1 is surrounded by a chain of six small islands and six hyperbolic fixed points: (*a*) Wigner function showing chain of six islands; (*b*) Husimi function showing that the island chain has been eliminated.

negative elliptic structures in between positive hyperbolic fixed points. And once again, the island chain has been removed in the Husimi distribution. Hence the unphysical 'negative probability' has been eliminated at the cost of removing structures which are real since they correspond to features of the classical Poincaré map.

3. Conclusion

The phase-space distributions for quantum states localized on the three main fixed points of the diamagnetic hydrogen Hamiltonian have been investigated numerically in the intermediate regime between integrability and full chaos, i.e. for $-1\leqslant\varepsilon<-0.1$. In addition, at the values of $\hbar\sim0.03$ considered here, scars are well localized on single states so only individual quantum states have been investigated. No energy smoothing has been carried out, but in principle it would be simple to consider superpositions of states or energy smoothed states.

The Wigner fringes of single states fill all of phase-space either due to the non-local nature of the Wigner function or the spread of ergodic trajectories. They are of a very different character in the chaotic/ergodic part of phase-space relative to fringes within stable islands, where the oscillations are regular and evenly spaced. In figures 4 and 5 one sees the large-scale structure of phase-space mapped out in a single state by relatively strong scar fringes on the one hand in the ergodic region and much weaker (by 10–1000 times) island fringes which resemble the Airy patterns of the regular regime. At this point the origin of the island fringes in a state dominated by the scar of a single unstable periodic orbit is unclear. They are similar to torus fringes yet are present even when there is no evident torus structure bordering them (e.g. Figure 5(*a*)).

Here no spatial smoothing has been carried out so it is worth comparing the results with Husimi distributions. Interesting classical features in individual Wigner functions, including weak scars, can be bordered by strong negative structures and hence may be

distorted or blurred by spatial smoothing. Features such as alternating positive/negative island chains are especially vulnerable and are not apparent in Husimi functions for the values of h considered here. It is also worth noting the differing typical length scales of the scar fringes (which have a wider variation of length scales) and the island fringes which are quite regularly spaced. This may make the latter more easily smoothed to zero. Plots of Husimi distributions for states localized mainly in the ergodic part of phase space, e.g. C and V1 (as in figures 4 and 5) show that the wavefunction is essentially absent inside the stable islands, while the Wigner function shows significant island fringes within these regions. So the Husimi distribution not only removes classically interesting features, but it also smooths out quantum fringes. Since the latter take a different form in stable regions from that in unstable regions they are also dynamically interesting.

Acknowledgments

The author gratefully acknowledges helpful discussions with Paul Dando, Wilfried Jans, Wolfgang Schweizer and Ken Taylor. The author also acknowledges support from SERC through fellowship AF/1298 and grant GR/H66099.

References

M S Bartlett and J E Moyal 1948 *Proc. Camb. Phil. Soc.* **45** 545
Berry M V 1977 *Phil. Trans. R. Soc. Lond.* A **287** 237
Berry M V 1989a *Proc. Roy. Soc. Lond.* A **423** 219
Berry M V 1989b *Proc. Roy. Soc. Lond.* A **424** 279
Clark C and Taylor K T 1982 *J. Phys. B: At. Mol. Phys.* **15** 1175
Dando P A, Monteiro T S, Schweizer W and Jans W 1993 *Rep. Theor. Phys.* submitted
Davies M J and Heller E J 1981 *J. Chem. Phys.* **75** 246
de Aguiar M A M, Ozorio de Almeida A M 1990 *J. Phys. A: Math. Gen.* **23** L1025
Friedrich H and Wintgen D 1989 *Phys. Rep.* **183** 37
Gutzwiller M C 1990 *Chaos in Classical and Quantum Mechanics* (New York: Springer-Verlag)
Hasegawa H, Robnik M and Wunner G 1990 *Prog. Theor. Phys.* supplement *Phys. Soc. Japan* **98** 198
Heller E J 1984 *Phys. Rev. Lett.* **53** 1515
Hillery M, O'Connell R F, Scully M O and Wigner E P 1984 *Phys. Rep.* **106** 121
Holle A, Main J, Wiebusch G, Rottke H and Welge K H 1988 *Phys. Rev. Lett.* **61** 161
Hutchinson J S and Wyatt R E 1980 *Chem. Phys. Lett.* **72** 378
Jans W, Monteiro T S, Schweizer W and Dando P 1993 *J. Phys. A: Math. Gen.* **26** 3187
Leboeuf P and Saraceno M 1990 *J. Phys. A: Math. Gen.* **23** 1745
Miller W H 1975 *J. Chem. Phys.* **663** 996
Monteiro T S 1992 *J. Phys. B: At. Mol. Opt. Phys.* **25** L621
Müller K, Hönig A and Wintgen D 1993 *Phys. Rev.* A **47** 3593
Müller K 1992 PhD thesis University of Heidelberg
Ozorio de Almeida A M and Hannay J H 1982 *Ann. Phys.* **138** 115
Schweizer W, Schaich M, Jans W, Wunner G and Ruder H 1993 preprint to be submitted
Schweizer W, Niemeier R, Friedrich H, Wunner G and Ruder H 1988 *Phys. Rev.* A **38** 1724
Schweizer W, Niemeier R, Wunner G and Ruder H 1993 *Z. Phys.* D **25** 95
Wigner E P 1932 *Phys. Rev.* **40** 749
Wintgen D and Friedrich H 1986 *J. Phys. B: At. Mol. Opt. Phys.* **19** 1261
Wintgen D and Friedrich H 1987 *Phys. Rev.* A **35** 1464